# Room-Temperature Creation and Spin−Orbit Torque Manipulation of Skyrmions in Thin Films with Engineered Asymmetry

Guoqiang Yu,[†] Pramey Upadhyaya,[†] Xiang Li,[†] Wenyuan Li,[†] Se Kwon Kim,[‡] Yabin Fan,[†] Kin L. Wong,[†] Yaroslav Tserkovnyak,[‡] Pedram Khalili Amiri,*,[†] and Kang L. Wang*,[†]
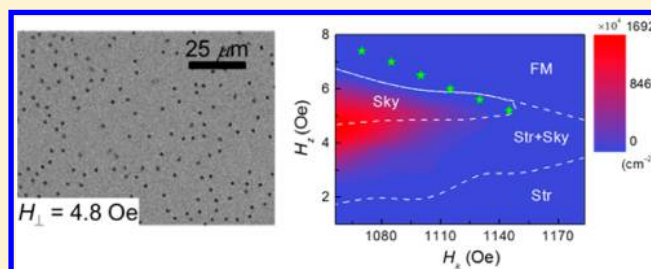
[†]Department of Electrical Engineering, University of California, Los Angeles, California 90095, United States
[‡]Department of Physics and Astronomy, University of California, Los Angeles, California 90095, United States

Ⓢ Supporting Information

**ABSTRACT:** Magnetic skyrmions, which are topologically protected spin textures, are promising candidates for ultralow-energy and ultrahigh-density magnetic data storage and computing applications. To date, most experiments on skyrmions have been carried out at low temperatures. The choice of available materials is limited, and there is a lack of electrical means to control skyrmions in devices. In this work, we demonstrate a new method for creating a stable skyrmion bubble phase in the CoFeB−MgO material system at room temperature, by engineering the interfacial perpendicular magnetic anisotropy of the ferromagnetic layer. Importantly, we also demonstrate that artificially engineered symmetry breaking gives rise to a force acting on the skyrmions, in addition to the current-induced spin−orbit torque, which can be used to drive their motion. This room-temperature creation and manipulation of skyrmions offers new possibilities to engineer skyrmionic devices. The results bring skyrmionic memory and logic concepts closer to realization in industrially relevant and manufacturable thin film material systems.

**KEYWORDS:** Skyrmion, room temperature, thin films, spin−orbit torque, symmetry breaking

Electrically controlled magnetic domain wall motion has been proposed as a mechanism of operation for ultrahigh-density and fast magnetic data storage (e.g., racetrack memory[1]) and logic devices. In this case, a bit of data is stored in a magnetic domain, confined by two adjacent domain walls, and is moved using spin polarized currents[1] or spin−orbit torques (SOTs).[2−5] Alternatively, the recently discovered magnetic skyrmion offers a different spin texture which can be similarly used for encoding data in memory and logic,[6−8] potentially resulting in significantly improved densities and much lower power dissipation compared to conventional domain wall devices.

A magnetic skyrmion is a swirling spin texture, which is topologically protected. Magnetic skyrmions were first observed in B20 compound materials, such as MnSi,[9−11] FeCoSi,[12,13] FeGe,[14] and $Cu_2OSeO_3$,[15,16] where they are induced by the bulk Dzyaloshinskii−Moriya interaction (DMI) due to the noncentrosymmetric crystal structure of these compounds.[17] On the other hand, ultrathin ferromagnetic transition metal films, when interfaced with a heavy metal with a large spin−orbit coupling, may also facilitate the creation of stable skyrmion states.[18−23] The implementation of skyrmions in thin film is of particular interest for applications, being suitable for room-temperature operation and compatible with existing semiconductor manufacturing tools. In contrast to bulk materials, however, skyrmions in thin films are induced by the interfacial DMI,[18,19,24] for which there is more choices of materials.

Compared with domain walls, the required current density for skyrmion displacement can be significantly lower,[11,25] making them particularly appealing for low-energy consumption spintronic memory and logic devices. Although a number of theoretical studies have shown that damping-like SOTs generated by electric currents can drive skyrmion motion in thin films of technological interest, few experiments have thus far demonstrated this type of skyrmion motion at room temperature.[21,23] Moreover, in these previous experiments, metastable skyrmions were *dynamically* created by either (i) nonuniform currents in a special geometry or (ii) by applying pulsed magnetic fields across the samples. The development of alternative methods of creating stable skyrmions at room temperature, which would lend themselves to design of practical devices, is thus particularly interesting for applications. Furthermore, there remains a need for detailed studies of room-temperature skyrmion dynamics driven by SOTs, in a setting relevant to practical device structures.

In this work, motivated by the above-mentioned needs, we report two new findings:
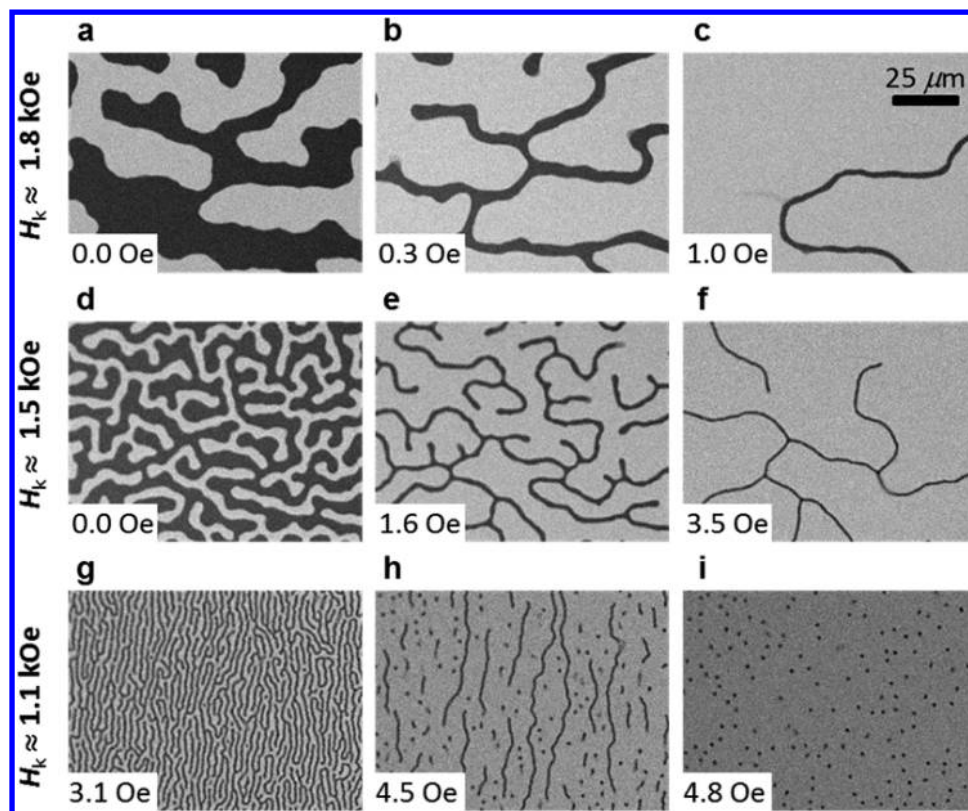
**Figure 1.** Evolution of magnetic domain patterns with perpendicular magnetic anisotropy ($H_k$). Polar-MOKE images of samples with perpendicular magnetic anisotropy fields of $H_k \approx 1.8$ kOe (a−c), 1.5 kOe (d−f), and 1.1 kOe (g−l) for different out-of-plane external magnetic field values. The $H_k \approx 1.8$ kOe and 1.5 kOe are within strong PMA regime and $H_k \approx 1.1$ kOe is within medium PMA regime. A lower $H_k$ value corresponds to a thicker Ta insertion layer. The bright (dark) areas represent $M_z > 0$ ($M_z < 0$).

First, we demonstrate a new method for creating a stable skyrmion bubble[26] phase in a Ta/$Co_{20}Fe_{60}B_{20}$(CoFeB)/MgO material system commonly used for magnetic memory applications, by engineering the interfacial perpendicular magnetic anisotropy (PMA) of the thin film. This is accomplished by inserting an ultrathin Ta layer between the CoFeB and the MgO. This method eliminates the need for the use of nonuniform currents or pulsed magnetic fields to create the skyrmions at room temperature. The interfacial DMI, due to the adjacent Ta heavy metal layer with a large spin−orbit coupling, facilitates the formation of the Néel-type chiral domain walls, and results in the creation of hedgehog-type skyrmions.

Second, we demonstrate that by breaking the lateral structural symmetry using an anisotropy gradient, an additional force can be engineered on the skyrmions, which can serve as a new control knob for skyrmionic devices. The skyrmion dynamics was studied in the presence of electric current-induced SOTs and this symmetry-breaking-induced force, which can be used to move skyrmions in functional devices such as racetracks or logic elements.[7,8] Moreover, all of the observations are made at room temperature, making them suitable for practical applications. Our work will open new opportunity for creating a class of new skyrmion devices.

**Results.** *I. Creating a Stable Skyrmion Phase in Thin Films through Anisotropy Engineering.* Previous experiments have demonstrated that a stable magnetic bubble phase can be created in magnetic thin films by modulating energy terms in the system (i.e., the magnetic anisotropy and Zeeman energy), e.g., by changing temperature and/or applying a magnetic

field.[27−30] Inspired by these previous experiments, one conceivable strategy for creating skyrmions is to add interfacial DMI into the created magnetic bubbles by interfacing the ferromagnetic layer with a heavy metal. The interfacial DMI, which is necessary to stabilize the chiral texture of the domain wall structures, is expected to give rise to a Néel-type chiral magnetic texture, turning the bubbles into hedgehog-type skyrmions with a nonzero topological number.

The film structure studied in this work consists of Ta (5)/ CoFeB (1)/ Ta (insertion layer with varying thickness across the wafer)/MgO (2)/ Ta (2) (thickness in nm), deposited by magnetron sputtering at room temperature on a thermally oxidized silicon substrate. The films were annealed at 250 °C for 30 min to enhance their PMA. The inserted Ta thickness is varied across the wafer to tune the PMA. Here, the role of the inserted Ta layer is to weaken the Fe−O and Co−O bonds at the interface, which in turn determine the magnitude of the interfacial perpendicular anisotropy.[31]

Figure 1a−i depict the evolution of magnetic domain patterns with different magnetic anisotropy, $H_k$, via different inserted Ta thicknesses under varying external magnetic fields. The images of magnetic domain patterns were captured by using a polar magneto-optical Kerr effect (MOKE) microscope.[21,32] The changes of domain patterns originate from the variation of the PMA, which decreases with the increasing Ta insertion thickness, as shown in Figure 2a. Three regions can be distinguished based on the magnitude of the perpendicular anisotropy:

(a) *Strong PMA regime* (e.g., $H_k = 1.8$ and 1.5 kOe): For films with a perpendicular anisotropy field $H_k$ of 1.8 kOe,
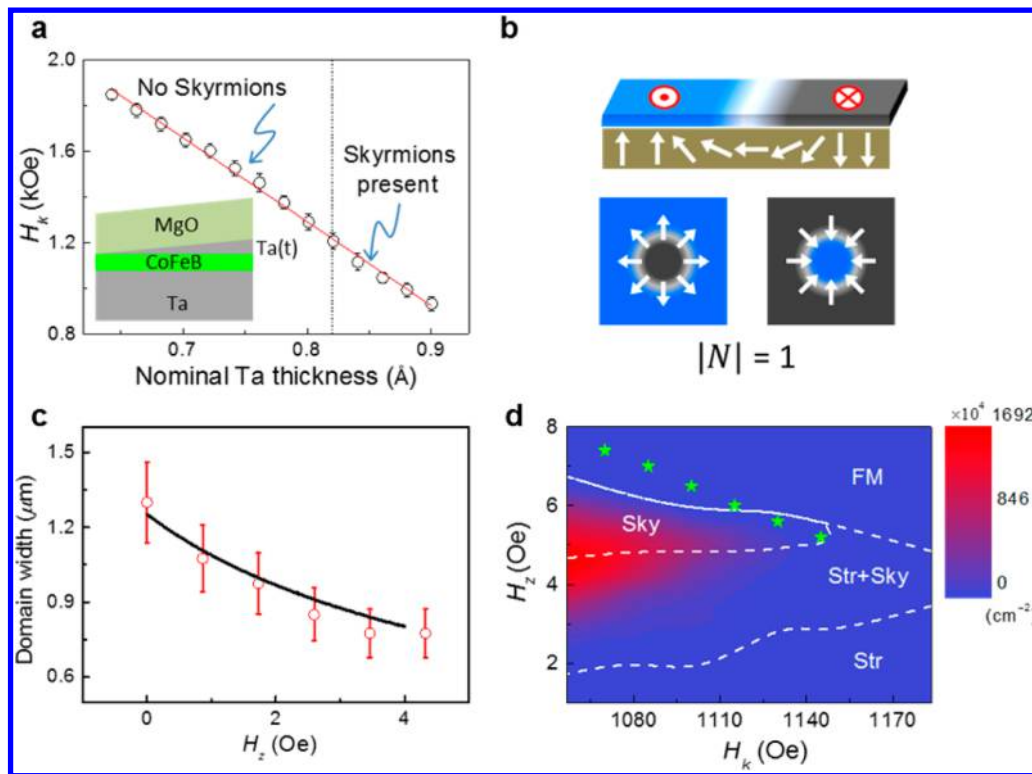
**Figure 2.** $H_k$ dependence on the inserted Ta thickness, the field dependence of the domain width, and the phase diagram of the magnetic structure. (a) The measured perpendicular magnetic anisotropy as a function of the inserted Ta thickness. The red line is the linear fit to the data. In the strong (medium) anisotropy regime (The two regimes are separated by the dashed line at $t = 0.82$ Å), skyrmions can (cannot) be observed when a proper $H_z$ is applied. The inset shows the sample structure. (b) Sketch of a Néel-type chiral domain wall (top) and skyrmion bubbles with Néel-type chiral circular domain walls. The topological charge number is 1. (c) Experimental domain width as a function of out-of-plane magnetic field ($H_z$). The black line shows the simulation results, from which the DMI is determined to be $|D| = 0.25$ mJ/m². (d) Phase diagram in the $H_z$ and $H_k$ plane. The color represents the skyrmion bubble density measured in a 233 $\mu$m × 174 $\mu$m area. The FM, Str, and Sky notations indicate the ferromagnetic, stripe, and skyrmion bubble phases, respectively. The dashed white lines show the boundaries between different phases. The green stars indicate the collapse fields for a single skyrmion bubble, which are estimated based on a theoretical model as detailed in supplementary section S2.

labyrinthine domains are observed at zero external magnetic field, as shown in Figure 1a. The formation of domain patterns originates from the competition among short-ranged exchange interaction, long-ranged dipole−dipole interaction, and the perpendicular magnetic anisotropy. When a positive out-of-plane magnetic field is applied, the favored domains ($M_z > 0$) expand in order to lower the Zeeman energy, while the other domains ($M_z < 0$) shrink, as shown in Figures 1b,c. Once the magnetic field reaches a critical value, the multidomain phase is transformed into a ferromagnetic phase, with all magnetic spins pointing in one direction. For smaller $H_k$, the domain size at zero field becomes smaller, as shown in Figure 1d.

(b) *Medium PMA regime* (e.g., $H_k = 1.1$ kOe): As the $H_k$ is further decreased to $H_k \approx 1.1$ kOe, an additional magnetic bubble phase appears between the labyrinthine domain phase and the ferromagnetic domain phase, as shown in Figures 1g−i. The diameters of the bubbles are ∼0.9 $\mu$m, which are also dependent on the external magnetic field. The stable bubble phase can be observed for $H_k < 1.2$ kOe, as shown in Figure 2a. The competition among the optimized anisotropy energy, dipole−dipole interaction, and Zeeman energy results in a stable bubble state. This is consistent with previous observations on bubble materials, such as doped variants of yttrium iron garnets.[33]

(c) *Weak PMA regime*: As the PMA is further reduced, eventually the equilibrium magnetization turns into the sample plane (not shown here), which however is not of interest in this work.

It is worth pointing out that, the Ta wedge insertion is used here but in general may not be necessary for the anisotropy modulation, and in principle other methods, e.g., strain- or voltage-induced anisotropy modulation,[34−37] can also be used for creating similar skyrmion bubble phases, and for controlling the boundaries between the above-mentioned strong, medium, and weak PMA regimes.

Next, we discuss the interfacial DMI magnitude in our samples, which favors Néel-like chiral domain walls[4] (as illustrated in the top schematic diagram in Figure 2b). The magnitude of the DMI is estimated by fitting the width of the narrow stripe domains as a function of out-of-plane magnetic field,[23] as shown in Figure 2c (see supplementary Section S1). In this manner, the DMI is determined to be 0.25 mJ/m², a value which indeed has been previously shown to be large enough for inducing Néel-type chiral domain walls in a Ta/CoFeB/MgO structure.[38,39] Therefore, the magnetization configurations of the bubbles are expected to be Néel-like skyrmions,[40] rather than topologically trivial ones. This is shown in the bottom schematic diagrams of Figure 2b, where the topological charges of the skyrmion bubble can be expressed as[6,17] $N = (1/4\pi)\int d^2r(\boldsymbol{m}\cdot\partial_x\boldsymbol{m} \times \partial_y\boldsymbol{m}) = \pm 1$. This is also consistent with the observed motion behavior of the bubbles when an in-plane current is applied to the sample, as will be discussed in Section II.
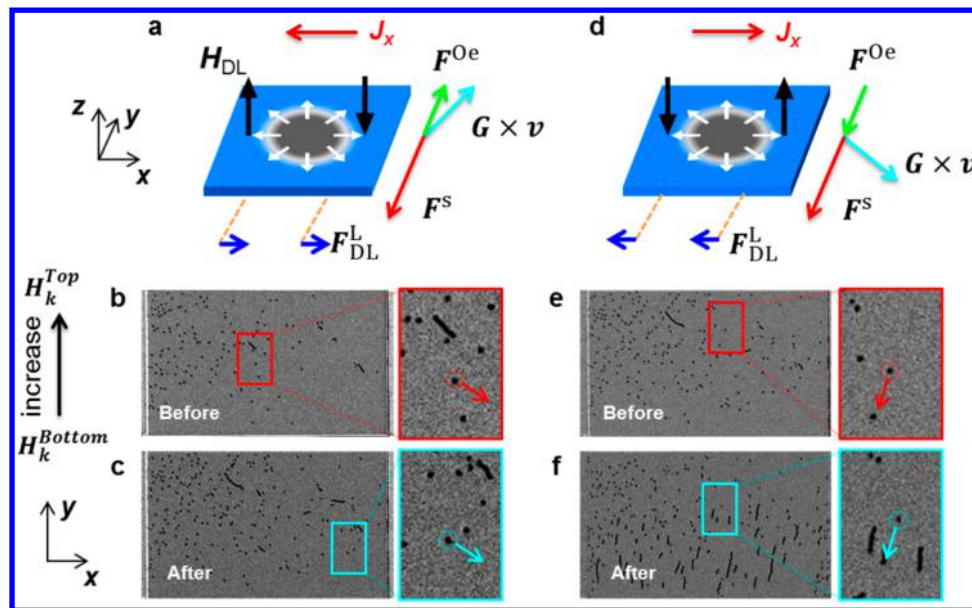
**Figure 3.** "Down" skyrmion bubble motion driven by currents in the $x$ direction that are perpendicular to $H_k$ gradient. a,d, The schematic diagrams for "down" skyrmion bubble motion driven by negative and positive currents, shown by red arrows. The area in blue (gray) represents $M_z > 0$ ($M_z <$ 0). The center magnetization in the domain wall is indicated by the white arrows. The effective fields corresponding to the damping-like torque ($H_{DL}$) on the side walls of the skyrmion bubbles are shown by black arrows. The direction of the four forces, $F_{DL}^L$, $F^s$, $F^{Oe}$, and $G \times v$, are shown by blue, red, green and light blue arrows. b,c,e,f, Images for skyrmion bubbles before and after 60 current pulses. The "down" skyrmion bubbles are driven by the current pulses ($J_x = 2.1 \times 10^6$ A/cm$^2$) at a constant out-of-plane magnetic field of $H_z = +5.0$ Oe. The red and light blue arrows label the skyrmion bubble being moved as example. The arrows show the motion direction. The rectangular areas on the right are magnified to clearly show the skyrmion bubble we follow, which is shown on the right side of each image. The $H_k$ value increases from the bottom to the top.

Next, the phase diagram for appearance of the skyrmion bubbles is shown in Figure 2d, based on the observed magnetic configurations as a function of the magnetic anisotropy and out-of-plane magnetic field. The general features of the phase diagram can be outlined below, followed by a discussion of the domain/skyrmion phase transition:

(i) At low magnetic fields, the magnetic film exhibits stripe domain patterns, corresponding to Figure 1g.

(ii) For a low $H_k$ value, a skyrmion phase will be favored as the magnetic field is increased (see Figure 1i). By changing the Zeeman energy (by increasing the magnetic field), the state is hence translated from a stripe domain phase to a skyrmion phase.

(iii) In the transition region between the stripe and skyrmion bubble phases, both stripes and skyrmion bubbles coexist (see Figure 1h).

(iv) When the magnetic field is further increased, the skyrmion bubble phase is eventually translated into a single-domain ferromagnetic phase.

(v) For a large enough value of $H_k$, the magnetic field range corresponding to stable skyrmions begins to shrink and eventually disappears, resulting in an abrupt transition from the stripe domain phase to a single-domain phase, without the appearance of skyrmion bubbles.

Theoretical calculations were carried out to understand the appearance of the skyrmion bubble phase (see Supplementary Section S2). The static magnetic energy for a single skyrmion bubble as a function of its radius is calculated including the DMI (see Figure S2). The estimated diameters of the bubble are in agreement with the experimental results (see Figure S3). In addition, the collapse fields, which correspond to the boundaries between the skyrmion bubble phase and the ferromagnetic phase, are also estimated based on the theoretical

model, as detailed in Supplementary Section S2. The results, including the measured DMI value (0.25 mJ/m$^2$), agree very well with the experimental results, as shown in Figure 2d. By contrast, without consideration of the DMI, the results deviate from our experimental results considerably (see Figure S4a). This comparison further confirms the reliability of the estimated DMI value, and its role in stabilizing the skyrmion phase in our samples. We would like to point out that the skyrmion sizes observed in this work are relatively large, which need to be further reduced for high-density data storage. The size could in principle be scaled down by carefully turning the material parameters, such as increasing the DMI value.[40]

*II. Current-Driven Skyrmion Motion.* Having established the skyrmion phase in equilibrium, we next turn to the manipulation of these skyrmion bubbles with electric currents using SOTs. In recent reports,[21,23] it was found that skyrmions can be moved by electric currents and the motion direction is along electron flow. In this work, we find that the equilibrium skyrmion bubbles are moved at angles with respect to the electron flow direction rather than simply along the electron flow direction. Moreover, the skyrmion motion angle is dependent on the electron flow direction and evolves with current density. A simple picture where the damping-like component of the SOT moves the DMI-stabilized Néel-like skyrmion bubbles is insufficient to qualitatively explain the measured transverse deflection angles. An additional force, induced by the lateral symmetry breaking due to the gradient of the inserted Ta between the CoFeB and MgO interfaces, needs to be involved in order to explain the observed skyrmion motion angles in the presence of current. We highlight the key experimental observations below.

The films were patterned into an array of two-terminal devices by standard photolithography and dry etching

techniques. The size of the two-terminal devices was fixed at 100 $\mu$m × 130 $\mu$m. The device channels were oriented along the direction of Ta thickness variation. Figure 3a−f illustrate the skyrmion motion driven by electric current. Figure 3a,d shows the skyrmion structure along with the collective coordinate forces for negative and positive currents, respectively. In Figures 3b,c and e,f, we show the experimental results of an applied current on the equilibrium structure of skyrmions stabilized by an out-of-plane external field of 5 Oe at $H_k$ = 1115 Oe, as described in Section I (see Figure 2d). First, one notes that the skyrmion bubbles are displaced by the electric current, as opposed to expanding or shrinking, indicating a chiral wall structure as expected.[21] However, different from previous studies,[21] the skyrmion bubbles move at an angle $\beta$ with respect to the electron current direction. A corresponding movie is provided in the Supporting Information, Section S3. The evolution of this angle $\beta$ with the magnitude of current is shown in Figure 4 (See Supplementary Section S4 for details on the method used for extraction of $\beta$). Two important observations can be made here:
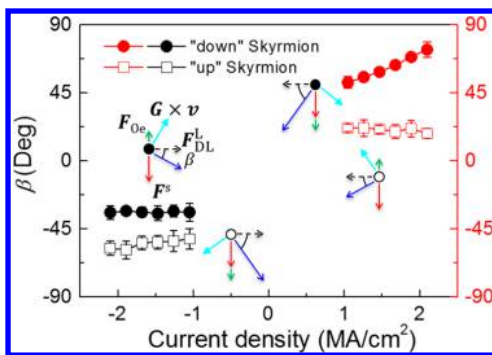


**Figure 4.** Current dependence of motion angle. The angle between the averaged skyrmion bubble motion direction (dark blue arrows) and the electron flow as a function of the current density, for the current direction perpendicular to the $H_k$ gradient. The solid circles and open squares represent "down" and "up" skyrmion bubbles. The red and black colors show the positive and negative current directions, which correspond to the right and left tick labels, respectively. The light blue, black dashed, red, and green arrows show the directions of the Lorentz force ($\mathbf{G} \times \mathbf{v}$), $F_{DL}^L$, $F^s$, and $F^T$, respectively.

(i) Although the velocity component along the current flow ($x$-axis) reverses upon reversing the direction of the current, the sign of the velocity component transverse to the current (along the $y$-axis) stays the same. In addition, the magnitude of the deflection angle $\beta$ is larger for one current direction than the other (see solid circles in Figure 4);

(ii) For the same current, $\beta$ is different for the "down" and "up" skyrmion bubbles (see Figures S6a−d and Figure 4), where the "down" ("up") configuration represents a skyrmion with its inner magnetization pointing down (up). Moreover, the magnitude and the current-dependence of $\beta$ remain approximately unchanged upon reversing *both* the current direction and the skyrmion core direction (up or down), while the sign of $\beta$ reverses.

We next present qualitative explanations of these observations, which provide evidence for the presence of a symmetry-breaking-induced force on the skyrmion bubbles.

We start by analyzing the motion of the skyrmion-bubbles using the collective coordinate approach[41,42] with the "rigid" translation approximation; i.e., where the coordinates of the

skyrmion's center are the only dynamic variables. In this case, the equation of motion for the skyrmion can be reduced to that of a massless particle satisfying the following force balance condition:[41]

$$\mathbf{G} \times \mathbf{v} - \Gamma\mathbf{v} + \mathbf{F}^I + \mathbf{F}^u = 0 \tag{1}$$

Here, the first term is the "Lorentz force", being nonzero for nontrivial topologies of the skyrmion bubbles as characterized by $\mathbf{G} = (0, 0, \mathcal{G})$, with $\mathcal{G} = -(M_s/\gamma) \int d^2r(m \cdot \partial_x m \times \partial_y m)$.[8] $M_s$ is the saturation magnetization and $\gamma$ is the gyromagnetic ratio. The integrand in $\mathcal{G}$ is the local solid angle, resulting in the integral being proportional to the number of times the magnetic configuration wraps a sphere in spin space, i.e., the same as the topological charge $N$. The second term in eq 1 is the "frictional" force due to the finite Gilbert damping, where $\Gamma = (\alpha M_s/\gamma) \int d^2r(\partial_x m \cdot \partial_x m) = \pm 1$ and $\alpha$ is the damping constant. The third term represents the force due to the applied current, which can include two contributions (i.e., $\mathbf{F}^I = \mathbf{F}_{DL} + \mathbf{F}_{Oe}$): One arising from the damping-like component of SOT, resulting from a mirror symmetry-breaking about the $xy$ plane,[43] whose components in the Cartesian coordinates are given by[4,5,32] $(F_{DL})_i = (\eta J M_s) \int d^2r(\partial_i m \cdot m \times (z \times j))$; and another force $\mathbf{F}_{Oe}$ originating from the Oersted-field gradient, which is always transverse to the current direction.[33] Here, $\eta$ parametrizes the strength of the damping-like component of the spin−orbit field, and $J$ and $j$ are the magnitude and the direction of the current density, respectively. Importantly, the magnitude and the direction of the SOT force depend on the details of the magnetic configuration of the wall. (This is also demonstrated experimentally in Supplementary Section S5, by looking at the SOT-induced skyrmion bubble translation, as opposed to its distortion, caused by the changes of its wall structure with an in-plane external magnetic field). Finally, the last term represents the force due to the changes in the potential energy of the skyrmion bubble as described by $\mathbf{F}^u = -\nabla U$, with the potential energy defined as $U(X, Y) = \int d^2r\mathcal{F}$, where $\mathcal{F}$ is the free energy density and $(X,Y)$ are the coordinates of the skyrmion.

Having discussed the possible forces acting on the skyrmion bubble, we are now ready to present qualitative explanations of the two key experimental observations mentioned above. First, we note that the scenario of skyrmion motion due to only the damping-like, Lorentz and Oersted gradient forces is not consistent with the experimental observations. This is because these forces, being odd functions of the current, must reverse upon reversing the current direction, hence resulting in the reversal of both components of the skyrmion's velocity. However, as noted in the observation (i) above (see Figures 3b,c and e,f), the velocity component transverse to the current does not change its sign upon reversing the current direction. This can be understood by performing a $\pi$-rotation transformation (i.e., simultaneous mirror transformations about the $xz$ and $yz$ planes), under which the magnetic configuration of a skyrmion bubble maps onto itself, but current and the velocity of the skyrmion reverse their directions. Thus, either of these mirror symmetries has to be broken in order to be consistent with the experimental observation. Indeed we note that the gradient in the Ta layer thickness along the $y$ axis direction (engineered for varying the strength of the perpendicular anisotropy, as discussed in Section II) breaks the mirror symmetry about the $xz$ plane. Consequently, we expect that a force ($\mathbf{F}^s$) due to its symmetry breaking will act on the

skyrmion bubble along the Ta wedge direction. Importantly, this force is independent of current direction. Such a symmetry breaking force is able to change the symmetry in the magnitude of $\beta$, resulting in a larger magnitude for positive currents, and smaller magnitude for negative currents, which is consistent with the observed experimental results. Based on the direction of skyrmion motion, the direction of $F^s$ is determined to be along the $-y$-axis.

Next we turn toward observation (ii), which is a manifestation of the fact that the "up" and "down" skyrmions transform into one another by a mirror transformation about the $yz$ plane, which, in turn, flips both the current and $\beta$ as shown in Figure S9. Within the force model of eq 1, this observation is consistent with the fact that the Lorentz force and $F_{Oe}$ reverse upon changing from the "up" skyrmion to the "down" case. This is because the Lorentz force reverses as the sign of the skyrmion number changes, and the Oersted-field gradient force, being coupled to the "dipole moment" of the skyrmion bubble, reverses between "up" and "down" skyrmions, as illustrated in Figure 4. At this point, we note that the wedge direction of the inserted Ta might be slightly misaligned with the $y$ axis, resulting in the slight observed deviation in the magnitude and current dependence of $\beta$ upon simultaneous reversal of current and skyrmion type. For comparison, we performed experiments in a device by rotating the film sample to align the gradient of anisotropy along the current direction during the fabrication. The corresponding results are discussed in the Supplementary Section S6, which can be similarly understood.

In principle, a quantitative fit to the deflection angles could be attempted using the force model discussed above. In fact, in the past experiments, where the skyrmions were moved by external magnetic field gradients, the skyrmion numbers have been quantitatively obtained from deflection angle measurements using the force model.[44] However, a quantitative analysis of *current-induced* motion of these skyrmion bubbles is complicated due to the dependence of $F_{DL}$ on the wall structure (as opposed to being independent of it for field-gradient driven motion), which is further discussed in the supplementary Section S7. This wall structure is both: (a) unknown (because of the competition of dipolar and DMI energy, at least for the sizes of skyrmion bubbles studied here), and (b) expected to evolve with current itself (for example due to the field-like component of the current-induced torque). In addition, the physical origin of the symmetry-breaking force $F^s$ is also not fully understood at this moment.

Neglecting the above-mentioned complications, one can attempt to quantitatively compare the observed deflection angles with the theory of an ideal Néel skyrmion bubble moving by the damping-like component of SOT, where the symmetry-breaking force is assumed to arise only due to the anisotropy-gradient-induced variation in the skyrmion's potential energy, i.e., $F^s = F^u$. We show the expected theoretical deflection angle in Figure S13, based on all force components calculated for a typically assumed Néel-like skyrmion bubble[40,45] (See Supplementary Section S8). As can be noted, the assumption of a Néel-like skyrmion bubble is not able to fully reproduce the measured angles, as shown in Figure S13, both qualitatively and quantitatively, for the whole range of currents studied here.

The possible reasons for this discrepancy between theory and experiments could arise from (a) neglecting the deviation from Néel-like skyrmion structure in the experiment, which could

significantly reduce the damping-like spin−orbit force (specially due to the large field-like component in the present samples). This is primarily due to the fact that the anisotropy gradient force is insignificant when compared with the damping-like and Lorentz forces for the case of a fixed Néel-like wall structure, which, however, is not expected to be the wall structure in our experiments; and/or (b) an additional source (different from the anisotropy-gradient-induced variation of the skyrmion's energy), contributing to the microscopic origin of the force induced by the lateral symmetry breaking, in combination with spin−orbit coupling at the ferromagnet/heavy metal interface. Indeed in previous experiments, such lateral symmetry breaking was shown to give rise to new phenomena and torques significantly affecting the switching behavior of perpendicular magnets, and resulting in the observation of zero-field SOT switching, which could not be purely understood in terms of an anisotropy energy gradient alone.[43]

In conclusion, we have demonstrated the creation of stable skyrmion bubbles in ultrathin CoFeB films at room temperature, by controlling their perpendicular magnetic anisotropy. The produced skyrmion bubble phase is stabilized from the competition among the short-ranged exchange interaction, long-ranged dipole−dipole interaction, and the perpendicular magnetic anisotropy. The presence of the interfacial DMI with a magnitude of 0.25 mJ/m$^2$ facilitates the Néel-type chiral property of the skyrmion domain walls. We further provided evidence of this chiral nature by demonstrating current-induced translational motion of the skyrmion bubbles. A detailed study of the deflection angle of the skyrmion bubbles revealed a driving force engineered via lateral symmetry, and suggested that the skyrmion wall structure might significantly affect the skyrmion motion under an applied current. It is hoped that these experimental findings will encourage more detailed theoretical studies of the wall structure (by varying competition of DMI and dipolar energy), including its deformations induced by the field-like component of the current-induced spin−orbit torque, along with the investigation of the possible microscopic mechanisms of the symmetry-breaking-induced force, which would be important for designing skyrmion-based spintronic devices.

## ■ ASSOCIATED CONTENT

### Ⓢ Supporting Information

The Supporting Information is available free of charge on the ACS Publications website at DOI: 10.1021/acs.nano-lett.5b05257.

> Additional information showing the determination of DMI strength, energy calculation for a single skyrmion, method for determining skyrmion motion direction, dependence of damping-like torque on wall structure, results for devices with wedge direction parallel to current direction, theoretical calculation of deflection angles, and characterization of torques (PDF)
> Movie for skyrmion motion (AVI)

## ■ AUTHOR INFORMATION

### Corresponding Authors
*E-mail address: pedramk@ucla.edu.
*E-mail address: wang@seas.ucla.edu.

### Author Contributions
G.Y. and P.U. contributed equally to this work.

## ◼ REFERENCES

(1) Parkin, S. S. P.; Hayashi, M.; Thomas, L. Magnetic domain-wall racetrack memory. *Science* **2008**, *320* (5873), 190.

(2) Miron, I.; Garello, K.; Gaudin, G.; Zermatten, P.; Costache, M.; Auffret, S.; Bandiera, S.; Rodmacq, B.; Schuhl, A.; Gambardella, P. Perpendicular switching of a single ferromagnetic layer induced by in-plane current injection. *Nature* **2011**, *476* (7359), 189.

(3) Liu, L.; Pai, C.; Li, Y.; Tseng, H.; Ralph, D.; Buhrman, R. Spin-Torque Switching with the Giant Spin Hall Effect of Tantalum. *Science* **2012**, *336* (6081), 555.

(4) Emori, S.; Bauer, U.; Ahn, S. M.; Martinez, E.; Beach, G. S. D. Current-driven dynamics of chiral ferromagnetic domain walls. *Nat. Mater.* **2013**, *12* (7), 611.

(5) Ryu, K.; Thomas, L.; Yang, S.; Parkin, S. Chiral spin torque at magnetic domain walls. *Nat. Nanotechnol.* **2013**, *8* (7), 527.

(6) Nagaosa, N.; Tokura, Y. Topological properties and dynamics of magnetic skyrmions. *Nat. Nanotechnol.* **2013**, *8* (12), 899.

(7) Fert, A.; Cros, V.; Sampaio, J. Skyrmions on the track. *Nat. Nanotechnol.* **2013**, *8* (3), 152.

(8) Upadhyaya, P.; Yu, G.; Amiri, P. K.; Wang, K. L. *Phys. Rev. B: Condens. Matter Mater. Phys.* **2015**, *92*, 134411.

(9) Muhlbauer, S.; Binz, B.; Jonietz, F.; Pfleiderer, C.; Rosch, A.; Neubauer, A.; Georgii, R.; Boni, P. Skyrmion Lattice in a Chiral Magnet. *Science* **2009**, *323* (5916), 915.

(10) Neubauer, A.; Pfleiderer, C.; Binz, B.; Rosch, A.; Ritz, R.; Niklowitz, P. G.; Boni, P. Topological Hall Effect in the A Phase of MnSi. *Phys. Rev. Lett.* **2009**, *102* (18), 186602.

(11) Jonietz, F.; Muhlbauer, S.; Pfleiderer, C.; Neubauer, A.; Munzer, W.; Bauer, A.; Adams, T.; Georgii, R.; Boni, P.; Duine, R. A.; et al. Spin Transfer Torques in MnSi at Ultralow Current Densities. *Science* **2010**, *330* (6011), 1648.

(12) Munzer, W.; Neubauer, A.; Adams, T.; Muhlbauer, S.; Franz, C.; Jonietz, F.; Georgii, R.; Boni, P.; Pedersen, B.; Schmidt, M. Skyrmion lattice in the doped semiconductor Fe1-xCoxSi. *Phys. Rev. B: Condens. Matter Mater. Phys.* **2010**, *81* (4), 041203.

(13) Yu, X. Z.; Onose, Y.; Kanazawa, N.; Park, J. H.; Han, J. H.; Matsui, Y.; Nagaosa, N.; Tokura, Y. Real-space observation of a two-dimensional skyrmion crystal. *Nature* **2010**, *465* (7300), 901.

(14) Yu, X. Z.; Kanazawa, N.; Onose, Y.; Kimoto, K.; Zhang, W. Z.; Ishiwata, S.; Matsui, Y.; Tokura, Y. Near room-temperature formation of a skyrmion crystal in thin-films of the helimagnet FeGe. *Nat. Mater.* **2011**, *10* (2), 106.

(15) Seki, S.; Yu, X. Z.; Ishiwata, S.; Tokura, Y. Observation of Skyrmions in a Multiferroic Material. *Science* **2012**, *336* (6078), 198.

(16) Onose, Y.; Okamura, Y.; Seki, S.; Ishiwata, S.; Tokura, Y. Observation of Magnetic Excitations of Skyrmion Crystal in a Helimagnetic Insulator Cu2OSeO3. *Phys. Rev. Lett.* **2012**, *109* (3), 037603.

(17) Rossler, U.; Bogdanov, A.; Pfleiderer, C. Spontaneous skyrmion ground states in magnetic metals. *Nature* **2006**, *442* (7104), 797.

(18) Heinze, S.; von Bergmann, K.; Menzel, M.; Brede, J.; Kubetzka, A.; Wiesendanger, R.; Bihlmayer, G.; Blugel, S. Spontaneous atomic-scale magnetic skyrmion lattice in two dimensions. *Nat. Phys.* **2011**, *7* (9), 713.

(19) Romming, N.; Hanneken, C.; Menzel, M.; Bickel, J. E.; Wolter, B.; von Bergmann, K.; Kubetzka, A.; Wiesendanger, R. Writing and Deleting Single Magnetic Skyrmions. *Science* **2013**, *341* (6146), 636.

(20) Dupe, B.; Hoffmann, M.; Paillard, C.; Heinze, S. Tailoring magnetic skyrmions in ultra-thin transition metal films. *Nat. Commun.* **2014**, *5*, 503010.1038/ncomms5030.

(21) Jiang, W.; Upadhyaya, P.; Zhang, W.; Yu, G.; Jungfleisch, M.; Fradin, F.; Pearson, J.; Tserkovnyak, Y.; Wang, K.; Heinonen, O.; et al. Blowing magnetic skyrmion bubbles. *Science* **2015**, *349* (6245), 283.

(22) Moreau-Luchaire, C.; Moutafis, C.; Reyren, N.; Sampaio, J.; Horne, N. V.; Vaz, C. A. F.; Bouzehouane, K. G.; Deranlot, C.; Warnicke, P.; Wohlhüter, P., et al.; *arXiv*:1502.07853, **2015**.

(23) Woo, S.; Litzius, K.; Krüger, B.; Im, M.-Y.; Caretta, L.; Kornel; Richter; Mann, M.; Krone, A.; Reeve, R., et al. Observation of room temperature magnetic skyrmions and their current-driven dynamics in ultrathin Co films. *arXiv*:1502.07376, **2015**.

(24) Bode, M.; Heide, M.; von Bergmann, K.; Ferriani, P.; Heinze, S.; Bihlmayer, G.; Kubetzka, A.; Pietzsch, O.; Blugel, S.; Wiesendanger, R. Chiral magnetic order at surfaces driven by inversion asymmetry. *Nature* **2007**, *447* (7141), 190.

(25) Yu, X. Z.; Kanazawa, N.; Zhang, W. Z.; Nagai, T.; Hara, T.; Kimoto, K.; Matsui, Y.; Onose, Y.; Tokura, Y. Skyrmion flow near room temperature in an ultralow current density. *Nat. Commun.* **2012**, *3*, 988.

(26) Here we use the term magnetic skyrmion or skyrmion bubble, specifically to denote the existence of a spin texture with chiral properties. This is distinguished from topologically trivial bubbles—stabilized by magnetostatic interactions in the absence of a significant DMI—which can also be present in thin films, without exhibiting the chiral properties observed in this work.

(27) Choi, J.; Wu, J.; Won, C.; Wu, Y. Z.; Scholl, A.; Doran, A.; Owens, T.; Qiu, Z. Q. Magnetic bubble domain phase at the spin reorientation transition of ultrathin Fe/Ni/Cu(001) film. *Phys. Rev. Lett.* **2007**, *98* (20), 207205.

(28) Wu, J.; Choi, J.; Won, C.; Wu, Y. Z.; Scholl, A.; Doran, A.; Hwang, C.; Qiu, Z. Q. Stripe-to-bubble transition of magnetic domains at the spin reorientation of (Fe/Ni)/Cu/Ni/Cu(001). *Phys. Rev. B: Condens. Matter Mater. Phys.* **2009**, *79* (1), 014429.

(29) Saratz, N.; Lichtenberger, A.; Portmann, O.; Ramsperger, U.; Vindigni, A.; Pescia, D. Experimental Phase Diagram of Perpendicularly Magnetized Ultrathin Ferromagnetic Films. *Phys. Rev. Lett.* **2010**, *104* (7), 077203.

(30) Saratz, N.; Ramsperger, U.; Vindigni, A.; Pescia, D. Irreversibility, reversibility, and thermal equilibrium in domain patterns of Fe films with perpendicular magnetization. *Phys. Rev. B: Condens. Matter Mater. Phys.* **2010**, *82* (18), 184416.

(31) Ikeda, S.; Miura, K.; Yamamoto, H.; Mizunuma, K.; Gan, H. D.; Endo, M.; Kanai, S.; Hayakawa, J.; Matsukura, F.; Ohno, H. A perpendicular-anisotropy CoFeB-MgO magnetic tunnel junction. *Nat. Mater.* **2010**, *9* (9), 721.

(32) Yu, G.; Upadhyaya, P.; Wong, K.; Jiang, W.; Alzate, J.; Tang, J.; Amiri, P.; Wang, K. Magnetization switching through spin-Hall-effect-induced chiral domain wall propagation. *Phys. Rev. B: Condens. Matter Mater. Phys.* **2014**, *89* (10), 104421.

(33) Malozemoff, A. P.; Slonczewski, J. C. *Magnetic Domain Walls in Bubble Materials*; Academic Press: New York, 1979.

(34) Weisheit, M. Electric field-induced modification of magnetism in thin-film ferromagnets (vol 315, pg 349, 1997). *Science* **2007**, *315* (5815), 1077.

(35) Maruyama, T.; Shiota, Y.; Nozaki, T.; Ohta, K.; Toda, N.; Mizuguchi, M.; Tulapurkar, A.; Shinjo, T.; Shiraishi, M.; Mizukami, S.;

et al. Large voltage-induced magnetic anisotropy change in a few atomic layers of iron. *Nat. Nanotechnol.* **2009**, *4* (3), 158.

(36) Liu, M.; Sun, N. Voltage control of magnetism in multiferroic heterostructures. *Philos. Trans. R. Soc., A* **2014**, *372* (2009), 20120439.

(37) Yu, G.; Wang, Z.; Abolfath-Beygi, M.; He, C.; Li, X.; Wong, K.; Nordeen, P.; Wu, H.; Carman, G.; Han, X. Strain-induced modulation of perpendicular magnetic anisotropy in Ta/CoFeB/MgO structures investigated by ferromagnetic resonance. *Appl. Phys. Lett.* **2015**, *106* (7), 072402.

(38) Emori, S.; Martinez, E.; Lee, K.; Lee, H.; Bauer, U.; Ahn, S.; Agrawal, P.; Bono, D.; Beach, G. Spin Hall torque magnetometry of Dzyaloshinskii domain walls. *Phys. Rev. B: Condens. Matter Mater. Phys.* **2014**, *90* (18), 184427.

(39) Torrejon, J.; Kim, J.; Sinha, J.; Mitani, S.; Hayashi, M.; Yamanouchi, M.; Ohno, H. Interface control of the magnetic chirality in CoFeB/MgO heterostructures with heavy-metal underlayers. *Nat. Commun.* **2014**, *5*, 565510.1038/ncomms5655.

(40) Sampaio, J.; Cros, V.; Rohart, S.; Thiaville, A.; Fert, A. Nucleation, stability and current-induced motion of isolated magnetic skyrmions in nanostructures. *Nat. Nanotechnol.* **2013**, *8* (11), 839.

(41) Thiele, A. Steady-State Motion of Magnetic Domains. *Phys. Rev. Lett.* **1973**, *30* (6), 230.

(42) Tretiakov, O.; Clarke, D.; Chern, G.; Bazaliy, Y.; Tchernyshyov, O. Dynamics of domain walls in magnetic nanostrips. *Phys. Rev. Lett.* **2008**, *100* (12), 127204.

(43) Yu, G.; Upadhyaya, P.; Fan, Y.; Alzate, J.; Jiang, W.; Wong, K.; Takei, S.; Bender, S.; Chang, L.; Jiang, Y.; et al. Switching of perpendicular magnetization by spin-orbit torques in the absence of external magnetic fields. *Nat. Nanotechnol.* **2014**, *9* (7), 548.

(44) Büttner, F.; Moutafis, C.; Schneider, M.; Krüger, B.; Günther, C. M.; Geilhufe, J.; Schmising, C. v. K.; Mohanty, J.; Pfau, B.; Schaffert, S.; et al. Dynamics and inertia of skyrmionic spin structures. *Nat. Phys.* **2015**, *11*, 225.

(45) Tomasello, R.; Martinez, E.; Zivieri, R.; Torres, L.; Carpentieri, M.; Finocchio, G. A strategy for the design of skyrmion racetrack memories. *Sci. Rep.* **2014**, *4*, 6784.